Quenching chatter instability in turning process with a vibro-impact nonlinear energy sink

Etienne Gourc, Sébastien Seguy, Guilhem Michon, Alain Berlioz, Brian Mann

Quenching chatter instability in turning process with a vibro-impact nonlinear energy sink

E. Gourc[a,], S. Seguy[b], G. Michon[c], A. Berlioz[d], BP. Mann[e]

[a] *Universidade Federal de Uberlandia, FEMEC, LMEst, Uberlândia, Brazil*
[b] *Université de Toulouse, Institut Clément Ader, INSA, Toulouse F-31077, France*
[c] *Université de Toulouse, Institut Clément Ader, ISAE, Toulouse F-31055, France*
[d] *Université de Toulouse, Institut Clément Ader, UPS, Toulouse F-31062, France*
[e] *Department of Mechanical Engineering and Materials Science, Duke University, Durham, NC 27708, USA*

Abstract

This paper investigates the passive control of chatter instability in turning processes using a vibro-impact nonlinear energy sink (NES). The workpiece is assumed to be rigid and the tool is flexible. A dynamical model including a nonlinear cutting law is presented and the stability lobes diagram are obtained. The behavior of the system with the vibro-impact NES is investigated using an asymptotic analysis. A control mechanism by successive beating is revealed, similarly to the strongly modulated response in the case of NES with cubic stiffness. It is shown that such a response regime may be beneficial for chatter mitigation. An original experimental procedure is proposed to verify the sizing of the vibro-impact NES. An experimental setup is developed with a vibro-impact NES embedded on the lathe tool and the results are analyzed and validated.

Keywords:
Chatter, instability, nonlinear energy sink, turning

1. Introduction

The surface quality of parts produced by machining operations is strongly affected by chatter. Chatter increases the surface roughness, tool wear and reduces the spindle lifespan. A possible model for this phenomenon is to consider the primary chatter. In this non resonant case, the coupling between two orthogonal cutting modes imply a pair of non-linear ordinary differential equations [1, 2]. Another modelization — improved and more used — is to consider the regenerative chatter. In this case, the instability is induced by the time-delay between two consecutive passages of the cutting teeth. Due to small disturbances, the lathe tool exhibit damped oscillations and the surface roughness is undulated. For consecutive workpiece revolutions, the chip thickness will be modulated.

Email addresses: etienne.gourc@gmail.com (E. Gourc), sebastien.seguy@insa-toulouse.fr (S. Seguy), guilhem.michon@isae.fr (G. Michon), alain.berlioz@univ-tlse3.fr (A. Berlioz), brian.mann@duke.edu (BP. Mann)

This mechanism, called the regenerative effect, has been first explained by Tobias and Fishwick [3] and is mainly responsible for chatter instability. Since these works, many researchers have improved the knowledge by the well known stability lobe representation and its application to special cases [4, 5, 6, 7, 8, 9, 10]. A detailed nonlinear analysis of chatter instability on turning processes has been carried out in [11] using the method of multiple scales.

Various techniques for chatter mitigation have been investigated. These different strategies may be divided in two categories, namely active and passive control. Concerning active vibration control strategies, a variable spindle speed was used in milling process to disturb the time delay [12]. The use of actively controlled piezzo-electric tools has been studied for turning processes [13], also the use of a piezoelectric tool holder was investigated theoretically and experimentally in [14]. Passive vibration strategies have also been investigated. Tuned mass damper has been widely studied for machining operations. Specific tuning procedure was developed for the case of chatter [15]. A nonlinear tuned mass damper with coulomb friction was analyzed for the case of turning in [16] and milling in [17], while multiple tuned mass damper were applied in [18].

In the past decade, it has been demonstrated that the addition of a small mass, strongly non-linear oscillator, called a nonlinear energy sink (NES), may lead to targeted energy transfer. In this context, a NES is used to mitigate any unwanted disturbance introduced in a primary system by efficiently transferring and eliminating energy from the main system to the NES. In [19], it was demonstrated that the main phenomena allowing targeted energy transfer is based on the $1:1$ resonance capture. When the primary system is subjected to harmonic forcing, the passive control acts through relaxation cycle, referred as strongly modulated response (SMR) [20]. This behavior has been confirmed experimentally in [21]. All these studies dealt with NES with cubic stiffness, however, this type of NES may not be suitable for practical applications, mainly due to its size. To overcome this problem, different types of NES have been proposed. Lamarque and co-workers analyzed a NES with piecewise linear stiffness [22, 23]. Vibro-impact NES for seismic mitigation have been studied numerically in [24] and experimentally in [25]. More recently, an analytical procedure based on the invariant manifold approach has been developed for a vibro-impact NES under impulse loading [26].

The aforementioned research on NES concern the passive control of linear system. The passive control of instability with NES is a growing interest. Reference [27] investigated the mitigation of limit cycle oscillations in a Van der Pol oscillator using a NES with cubic stiffness. It was shown analytically that the system exhibits three control mechanisms, namely: suppression, stabilization and passive control through SMR. The case of a rigid airfoil in an air flow has been treated theoretically and experimentally in [28, 29]. A similar case has been analyzed by Vaurigaud [30], where a long bridge in which flutter may occur is considered. The use of a NES has also been investigated in [31] to passively control instabilities that may occur during drilling operations for oil and gas. The passive control of chatter instability, using a NES with cubic stiffness, has been explored in [32]. The same three mechanism, as those found for the Van der Pol oscillator [27], have been evidenced. A refined model taking into account the loss of contact of the tool during high amplitude oscillations has been studied in [33].

The goal of the present paper is to investigate theoretically and experimentally the potential benefit of a vibro-impact NES to passively control chatter instability in a turning process. The system is composed of a flexible lathe tool on which a NES is embed-

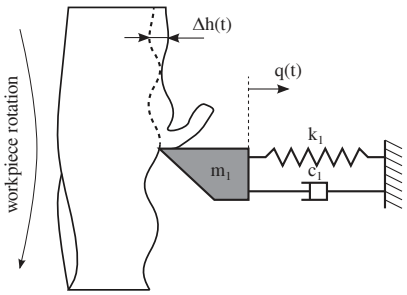

Figure 1: Schematic representation of the turning process.

ded. The structure of the paper is as follows. The second section describes a model of a turning process. The linearized system is analyzed in section 3. Section 4 provides a theoretical analysis of the coupled system and a description of the response regimes. Section 5 describes of the experimental setup. The tuning of the vibro-impact NES and time history of the experimental measurements are also presented. Section 6 contains concluding remarks and discussion.

2. Modelization of turning process

The uncoupled system consists of a flexible lathe tool which is assumed to vibrate only in its first bending mode, perpendicular to the cutting direction. It has been shown that the bending mode in the direction parallel to the cutting direction play an insignificant role [34]. The workpiece is assumed to be rigid. A schematic representation of this system is given in Fig. 1 and the corresponding equation of motion is written as follows

$$m_1 \frac{d^2q}{dt^2} + c_1 \frac{dq}{dt} + k_1 q = F_c \tag{1}$$

where q represent the tool tip displacement, m_1, k_1 and c_1 represent the modal mass, stiffness and damping of the first bending mode, respectively. The cutting force takes into account the regenerative effect and is expressed in polynomial form as follows [35]

$$F_c\left(\Delta h(t)\right) = p\left(\rho_1 h(t) + \rho_2 h(t)^2 + \rho_3 h(t)^3\right) \tag{2}$$

where p is the depth of cut, $h(t)$ represents the instantaneous chip thickness and ρ_i $(i = 1..3)$ are the specific cutting coefficients obtained from experimental measurements. Typical values of these coefficients for steel cutting are given in [36]. The instantaneous chip thickness may be expressed as follows

$$h(t) = h_0 + \Delta h(t) \tag{3}$$

here, h_0 is the nominal chip thickness without vibration and $h(t)$ represents the chip thickness variation which depends on the instantaneous position of the tool tip, and the position of the tool tip from the previous workpiece rotation, as illustrated in Fig. 1. It is expressed as

$$\Delta h(t) = q(t-\tau) - q(t) \tag{4}$$

where $q(t-\tau)$ is the delayed position of the tool. τ is the time delay between two successive tool passages, which corresponds to the period of one workpiece rotation $\tau = 2\pi/\Omega$ (Ω is the workpiece angular speed). When the cutting process is stable, $q(t) = q_0$. Substituting Eq. (3) into (1) gives

$$k_1 q_0 = p\left(\rho_1 h_0 + \rho_2 h_0^2 + \rho_3 h_0^3\right) \tag{5}$$

During unsteady regimes, the displacement is the sum of the steady component q_0 and an unsteady component $u(t)$

$$q(t) = q_0 + u(t) \tag{6}$$

Substituting Eqs. (5,6) into (1) give

$$m_1 \frac{d^2u}{dt^2} + c_1 \frac{du}{dt} + k_1 u = p\left(\alpha_1 \Delta\tilde{h} + \alpha_2 \Delta\tilde{h}^2 + \alpha_3 \Delta\tilde{h}^3\right) \tag{7}$$

where $\Delta\tilde{h} = u(t-\tau) - u(t)$, $\alpha_1 = 2\rho_2 h_0 + 3\rho_3 h_0^2 + \rho_1$, $\alpha_2 = 3\rho_3 h_0 + \rho_2$ et $\alpha_3 = \rho_3$. The following changes of variables are introduced

$$\begin{array}{l} T = \omega_1 t, \quad \omega_1^2 = \dfrac{k_1}{m_1}, \quad 2\mu_1 = \dfrac{c_1}{m_1\omega_1}, \\ \psi = \dfrac{p\alpha_1}{m_1\omega_1^2}, \quad \eta_1 = \dfrac{p\alpha_2}{\psi m_1\omega_1^2}, \quad \eta_2 = \dfrac{p\alpha_3}{\psi m_1\omega_1^2} \end{array} \tag{8}$$

After substitution of (8) into (7) we obtain

$$\ddot{u} + 2\mu_1\dot{u} + u = \psi\left(\Delta\tilde{h} + \eta_1\Delta\tilde{h}^2 + \eta_2\Delta\tilde{h}^3\right) \tag{9}$$

where the dot represents the differentiation with respect to the non-dimensional time T.

3. Analysis of the linearized system

After removing the nonlinear terms in the cutting law by setting $\eta_1 = \eta_2 = 0$ in Eq. (9), the linearized equation of motion of the cutting tool is given by

$$\ddot{u} + 2\mu_1\dot{u} + u + \psi\left(u(T-\tau) - u(T)\right) = 0 \tag{10}$$

The solution of (10) can be written by

$$u = u_0 \mathrm{e}^{(\gamma + i\omega)t} \tag{11}$$

where γ is the grow or decay rate, ω is the pulsation of the oscillations and u_0 depends on the initial conditions. After substituting Eq. (11) into (10), we obtain

$$\psi\left(1 - \mathrm{e}^{(\gamma+i\omega)\tau}\right) + (\gamma + i\omega)^2 + 2\mu_1(\gamma + i\omega) + 1 = 0 \tag{12}$$

After splitting Eq. (12) into real and imaginary parts, the following equations were obtained:

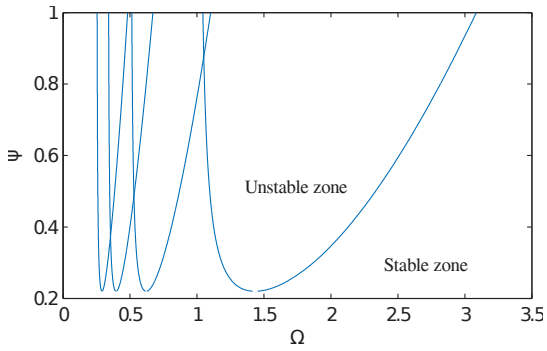

Figure 2: Example of stability lobes diagram.

$$\begin{aligned} &\psi\left(1-\cos(\omega\tau)\mathrm{e}^{-\gamma\tau}\right)+\gamma^2-\omega^2+2\mu_1\gamma+1=0\\ &\psi\sin(\omega\tau)\mathrm{e}^{-\gamma\tau}+2\omega\left(\gamma+\mu_1\right)=0 \end{aligned} \tag{13}$$

When $\gamma > 0$, the amplitude of the oscillations growth exponentially and the system is unstable. On the contrary, when $\gamma < 0$, the amplitude of the oscillations decay with time and the turning process is stable. In order to evaluate the stability boundary, we set $\gamma = 0$ in Eq. (13)

$$\begin{aligned} &\psi\cos(\omega\tau)=\psi-\omega^2+1\\ &\psi\sin(\omega\tau)=-2\mu_1\omega \end{aligned} \tag{14}$$

Using trigonometric identity in (14), the pulsation of the bifurcated solution (also called chatter frequency) is obtained as

$$\omega = 1+\psi-2\mu_1^2 \pm \sqrt{-4\mu_1^2+\left(\psi-2\mu_1^2\right)^2} \tag{15}$$

It is possible to prove that the bifurcation $(\gamma, \psi, \omega) = (0, \psi_c, \omega_c)$ is a Hopf bifurcation [11]. For practical machining applications, the stability boundary is often plot in the space of parameters (Ω, ψ) and is called the stability lobe diagram. An example of such a diagram is depicted in Fig. 2. The turning process is stable for cutting conditions under the lobes and is unstable otherwise.

4. Passive control of chatter instability using a vibro-impact NES

In this section, the dynamics of the lathe tool coupled with the vibro-impact NES is investigated. A schematic representation of the coupled system is given in Fig. 3. The corresponding dimensionless equations of motion between impact, after eliminating the static deflection are written as follow

$$\begin{aligned} &\ddot{u}+2\mu_1\dot{u}+u=\psi\left(\Delta\tilde{h}+\eta_1\Delta\tilde{h}^2+\eta_2\Delta\tilde{h}^3\right)\\ &\epsilon^2\ddot{y}=0, \forall|ru-y|<\Delta \end{aligned} \tag{16}$$

where y represents the absolute displacement of the free mass of the vibro-impact NES, $\epsilon^2 = m_2/m_1 \ll 1$ represent the mass ratio between the modal mass of the tool and the

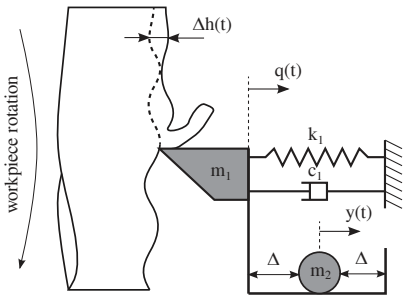

Figure 3: Schematic representation of the passive control of chatter instability using a vibro-impact NES.

mass of the vibro-impact NES, Δ represents the gap between the free mass and the rigid walls and r is an influence coefficient depending of the position of the vibro-impact NES on the tool. The impacts are modelled using the Newton coefficient of restitution on velocities and the condition of conservation of momentum as follow

$$\begin{aligned} &u_+ = u_-, \quad y_+ = y_- \\ &r\dot{u}_+ - \dot{y}_+ = -R\left(r\dot{u}_- - \dot{y}_-\right) \\ &\dot{u}_+ + \epsilon^2\dot{y}_+ = \dot{u}_- + \epsilon^2\dot{y}_- \\ &\text{for } |ru - y| = \Delta \end{aligned} \tag{17}$$

here, the subscripts $+$ and $-$ represent the time immediately after and before impact and R is the coefficient of restitution ($R \in [0, 1]$).

4.1. Asymptotic analysis

The following algebraic developments have been carried out using the computer algebra software Maple. Equations (16) and (17) are analyzed using the method of multiple scales. New coordinates are introduced as follow

$$v = u + \epsilon^2 y, \quad w = ru - y \tag{18}$$

where v and w represents the displacement of the center of mass and the internal displacement of the vibro-impact NES, respectively. After substituting Eqs. (18) into Eqs. (16,17), it follows

$$\begin{aligned} &\ddot{v} + 2\mu_1 \frac{\dot{v} + \epsilon^2\dot{w}}{1 + r\epsilon^2} + \frac{v + \epsilon^2 w}{1 + r\epsilon^2} = \psi\left[\frac{v_\tau + \epsilon^2 w_\tau}{1 + r\epsilon^2} - \frac{v + \epsilon^2 w}{1 + r\epsilon^2}\right. \\ &\left.+\eta_1\left(\frac{v_\tau + \epsilon^2 w_\tau}{1 + r\epsilon^2} - \frac{v + \epsilon^2 w}{1 + r\epsilon^2}\right)^2 + \eta_2\left(\frac{v_\tau + \epsilon^2 w_\tau}{1 + r\epsilon^2} - \frac{v + \epsilon^2 w}{1 + r\epsilon^2}\right)^3\right] \\ &\frac{r\ddot{v} - \ddot{w}}{1 + r\epsilon^2} = 0, \quad \forall |w| < \Delta \end{aligned} \tag{19}$$

$$\begin{aligned} &v_+ = v_-, \quad w_+ = w_- \\ &\dot{w}_+ = -R\dot{w}_-, \quad \dot{v}_+ = \dot{v}_- \\ &\text{for } |w| = \Delta \end{aligned} \tag{20}$$

here $v_\tau = v(t-\tau)$ and $w_\tau = w(t-\tau)$. Since secular terms first appear at $O(\epsilon^3)$, a detuning parameter representing the vicinity of ψ to ψ_c is introduced as follow [11]

$$\psi = \psi_c + \epsilon^2 \sigma \tag{21}$$

The solutions of Eqs (19,20) are expanded in power series as

$$\begin{aligned} v(T;\epsilon) &= \epsilon v_1(T_0,T_1,T_2) + \epsilon^2 v_2(T_0,T_1,T_2) + \epsilon^3 v_3(T_0,T_1,T_2) + \dots \\ w(T;\epsilon) &= \epsilon w_1(T_0,T_1,T_2) + \epsilon^2 w_2(T_0,T_1,T_2) + \epsilon^3 w_3(T_0,T_1,T_2) + \dots \end{aligned} \tag{22}$$

where $T_n = \epsilon^n T$ $(n = 0, 1, \dots)$. The time delay is considered to be of $O(1)$, which is rather natural if the behavior close to the order 0 lobe is analyzed. In this case, the delayed position of the tool and the vibro-impact NES are written as

$$\begin{aligned} v(T-\tau;\epsilon) &= \epsilon v_1(T_0-\tau,T_1,T_2) + \epsilon^2 \left(v_2(T_0-\tau,T_1,T_2) - \tau D_1 v_1(T_0-\tau,T_1,T_2)\right) \\ &+\epsilon^3 \Bigg(v_3(T_0-\tau,T_1,T_2) + \frac{\tau^2}{2} D_1^2 v_1(T_0-\tau,T_1,T_2) - \tau D_2 v_1(T_0-\tau,T_1,T_2) \\ &\qquad -\tau D_1 v_2(T_0-\tau,T_1,T_2)\Bigg) + \dots \\ w(T-\tau;\epsilon) &= \epsilon w_1(T_0-\tau,T_1,T_2) + \epsilon^2 \left(w_2(T_0-\tau,T_1,T_2) - \tau D_1 w_1(T_0-\tau,T_1,T_2)\right) \\ &+\epsilon^3 \Bigg(w_3(T_0-\tau,T_1,T_2) + \frac{\tau^2}{2} D_1^2 w_1(T_0-\tau,T_1,T_2) - \tau D_2 w_1(T_0-\tau,T_1,T_2) \\ &\qquad -\tau D_1 w_2(T_0-\tau,T_1,T_2)\Bigg) + \dots \end{aligned} \tag{23}$$

Substituting Eqs. (22,23) into Eqs. (19,20) and equating coefficients of like power of ϵ, it comes

$$\begin{aligned} \epsilon^1 : \quad & D_0^2 v_1 + 2\mu_1 D_0 v_1 + v_1 - \psi_c \left(v_{1\tau} - v_1\right) = 0 \\ & D_0^2 w_1 - r D_0^2 v_1 = 0, \quad \forall |w_1| < \Delta \\ & v_{1+} = v_{1-}, \quad w_{1+} = w_{1-} \\ & D_0 v_{1+} = D_0 v_{1-}, \quad D_0 w_{1+} = -R D_0 w_{1-}, \quad \text{for } |w_1| = \Delta \end{aligned} \tag{24}$$

$$\begin{aligned} \epsilon^2 : \quad & D_0^2 v_2 + 2\mu_1 D_0 v_2 + v_2 - \psi_c \left(v_{2\tau} - v_2\right) = -2\mu_1 D_1 v_1 - 2 D_0 D_1 v_1 \\ & \qquad -\psi_c \tau D_1 v_{1\tau} + \psi_c \eta_1 \left(v_{1\tau} - v_1\right)^2, \quad \forall |w_2| < \Delta \\ & v_{2+} = v_{2-}, \quad w_{2+} = w_{2-} \\ & D_0 v_{1+} + D_0 v_{2+} = D_0 v_{1-} + D_0 v_{2-}, \\ & D_0 w_{1+} + D_0 w_{2+} = -R \left(D_0 w_{1-} + D_0 w_{2+}\right), \text{for } |w_2| = \Delta \end{aligned} \tag{25}$$

$$
\epsilon^3:\quad
\begin{aligned}
&D_0^2 v_3 + 2\mu_1 D_0 v_3 + v_3 - \psi_c\left(v_{3\tau} - v_3\right) = 2\mu_1\left(rD_0 v_1 - D_1 v_2 - D_2 v_1 - D_0 w_1\right)\\
&+2\psi_c\eta_1\left(v_1 - v_{1\tau}\right)\left(D_1 v_{1\tau} - v_{2\tau} + v_2\right) - \psi_c\eta_2\left(v_1 - v_{1\tau}\right)^3 + \psi_c r\left(v_1 - v_{1\tau}\right)\\
&+\psi_c\left(w_{1\tau} - w_1 + \frac{\tau^2}{2}D_1^2 v_{1\tau} - \tau D_1 v_{2\tau} - D_2 v_{1\tau}\right) + v_1 r - w_1 - 2D_0 D_1 v_2 - 2D_0 D_2 v_1\\
&-D_1^2 v_1 + \sigma\left(v_{1\tau} - v_1\right), \quad \forall |w_3| < \Delta\\
&v_{3+} = v_{3-}, \quad w_{3+} = w_{3-}\\
&D_0 v_{1+} + D_0 v_{2+} + D_0 v_{3+} = D_0 v_{3-} + D_0 v_{2-} + D_0 v_{3-},\\
&D_0 w_{1+} + D_0 w_{2+} + D_0 w_{3+} = -R\left(D_0 w_{1-} + D_0 w_{2+} + D_0 w_{3+}\right), \text{for } |w_3| = \Delta
\end{aligned}
\tag{26}
$$

The other equations at order ϵ^2 and ϵ^3 are not given because they are not used in the following analysis.

4.1.1. Order ϵ^1

The solution of the first equation of (24) may be written as follow [11]

$$
v_1 = A\mathrm{e}^{i\omega_c T_0} + \sum_{m=1}^{\infty} A_m \mathrm{e}^{(\gamma_m + i\omega_m)T_0} + cc \tag{27}
$$

Where ω_c is the critical chatter frequency corresponding to $\sigma = 0$, obtained using 15. Close to the stability boundary, all the remaining roots $\gamma_m \pm i\omega_m$ have negative real part and decay with time. Thus, the long time behavior is expressed by

$$
v_1 = A\mathrm{e}^{i\omega_c T_0} + cc \tag{28}
$$

where cc denotes the complex conjugate of the preceding terms. Substituting (28) into the second equation of (24), gives

$$
\begin{aligned}
&D_0^2 w_1 + r\omega_c^2\left(A\mathrm{e}^{i\omega_c T_0} + \bar{A}\mathrm{e}^{-i\omega_c T_0}\right), \quad \forall |w_1| < \Delta\\
&w_{1+} = w_{1-}, \quad D_0 w_{1+} = -RD_0 w_{1-}, \quad \text{for } |w_1| = \Delta
\end{aligned}
\tag{29}
$$

This equation corresponds to a harmonically forced vibro-impact oscillator. Between impact (i.e. when $|w_1| < \Delta$), the solution of (29) is given by

$$
w_1 = r\left(A\mathrm{e}^{i\omega_c T_0} + \bar{A}\mathrm{e}^{-i\omega_c T_0}\right) + BT_0 + C \tag{30}
$$

Like 1 : 1 resonance capture between the lathe tool and the vibro-impact NES is assumed, we consider solutions with two symmetric impacts per cycle. The periodicity conditions on a half period are written as follow

$$
w_1\left(\frac{\pi}{\omega_c}\right) = -w_1(0), \quad D_0 w_{1+}\left(\frac{\pi}{\omega_c}\right) = -D_0 w_{1+}(0) \tag{31}
$$

The solution between impact given by Eq. (30) together with the periodicity conditions in Eq. (31) are used to recover the integration constants B and C. At time $T_0 = 0$, it is assumed that the free mass of the vibro-impact NES is in contact with the left side of the cavity

$$w_1(0) = \Delta \tag{32}$$

Substituting Eq. (30) into the first periodicity condition in (31) yields

$$B = -\frac{2C\omega_c}{\pi} \tag{33}$$

After substituting Eq. (30) into the second periodicity condition in Eq. (31) and in (32), the following relations are obtained

$$\begin{array}{l} r\omega_c i\left(A - \bar{A}\right)(1+R) + B\,(1-R) = 0 \\ r\left(A + \bar{A}\right) + C - \Delta = 0 \end{array} \tag{34}$$

Substituting relation (33) into (34) and introducing polar form $A = a\mathrm{e}^{i\alpha}$ it follows

$$\sin\alpha = \frac{C\delta}{ra\pi}, \quad \cos\alpha = -\frac{C-\Delta}{2ra} \tag{35}$$

where $\delta = (R-1)/(R+1)$. Using trigonometric identity in (35) yields

$$a^2 = \frac{C^2\delta^2}{r^2\pi^2} + \frac{(C-\Delta)^2}{4r^2} \tag{36}$$

Equation (36) represents the slow invariant manifold (SIM) of the problem at time scale T_1 when the vibro-impact NES oscillate with two symmetric impacts per period of oscillation of the lathe tool [26]. The SIM admit an extremum computed by vanishing the derivative of the right hand side of (36) with respect to C

$$C_{min} = \frac{\pi^2\Delta}{4\delta^2 + \pi^2}, \quad a^2_{min} = \frac{\Delta^2\delta^2}{r^2\left(4\delta^2 + \pi^2\right)} \tag{37}$$

Equation (37) is of particular interest since it represents the minimum amplitude of the lathe tool which allow the vibro-impact NES to vibrate in regimes with two symmetric impacts per cycle. The analysis of the stability of the SIM is not trivial due to the discontinuities in the velocities and requires analyzing the Poincaré section of the perturbed system [37, 38]. The perturbed solutions of Eq. (29) are written as follow

$$\begin{array}{ll} \tilde{w}_1 = \tilde{A}\mathrm{e}^{i\omega_c T_0} + \bar{\tilde{A}}\mathrm{e}^{-i\omega_c T_0} + \tilde{B}_1 T_0 + C_1, & 0 < T_0 < t_1 \\ \tilde{w}_1 = \tilde{A}\mathrm{e}^{i\omega_c T_0} + \bar{\tilde{A}}\mathrm{e}^{-i\omega_c T_0} + \tilde{B}_2 T_0 + C_2, & t_1 \leq T_0 < t_e \end{array} \tag{38}$$

where $t_1 = \pi/\omega_c + \Delta t_1$, $t_e = 2\pi/\omega_c + \Delta t_1 + \Delta t_2$ and $\tilde{A}$ takes into account a phase perturbation as

$$\tilde{A} = a\mathrm{e}^{i\alpha + \Delta\alpha} \tag{39}$$

The initial conditions of the perturbed system are given by

$$\tilde{w}_1(0) = \Delta, \quad D_0\tilde{w}_1(0) = D_0 w_1(0) + \Delta\dot{w} \tag{40}$$

and the periodicity conditions of the perturbed system are expressed as

$$\begin{array}{l} \tilde{w}_1(t_1) = -\tilde{w}_1(0), \quad D_0\tilde{w}_1(t_{1+}) = -D_0\tilde{w}_1(0_+), \\ \tilde{w}_1(t_e) = \tilde{w}_1(0), \quad D_0\tilde{w}_1(t_{e+}) = D_0\tilde{w}_1(0_+) \end{array} \tag{41}$$

Substituting the solutions of the perturbed system given in Eq. (38) into (40,41) and solving for B_i and C_i $(i = 1, 2)$, it comes

$$\begin{array}{l} B_1 = 2ra\omega_c \sin(\alpha + \Delta\alpha) + D_0 w_1(0) + \Delta\dot{w} \\ C_1 = -2ra\cos(\alpha + \Delta\alpha) + \Delta \\ B_2 = 2ra\omega_c(1+R)\sin(\alpha + \Delta\alpha + \omega_c t_1) - RB_1 \\ C_2 = -2t_1 ra\omega_c(1+R)\sin(\alpha + \Delta\alpha + \omega_c t_1) + t_1(1+R)B_1 + C_1 \end{array} \tag{42}$$

The computed Poincaré section for solutions with two symmetric impacts per cycle is obtained

$$\begin{array}{l} \Delta\dot{w}' = D_0\tilde{w}_{1+}(t_e) - D_0 w_1(0_+) \equiv f_1(\Delta\dot{w}, \Delta\alpha) \\ \Delta\alpha' = \Delta\alpha + \Delta t_1 + \Delta t_2 \equiv f_2(\Delta\dot{w}, \Delta\alpha) \end{array} \tag{43}$$

The stability of the SIM is determined by the location of the eigenvalues of the Jacobian matrix with respect to the unit circle. The Jacobian matrix of the linearized system is written as follow

$$J = \begin{bmatrix} \dfrac{\partial f_1}{\partial \Delta\dot{w}} & \dfrac{\partial f_1}{\partial \Delta\alpha} \\ \dfrac{\partial f_2}{\partial \Delta\dot{w}} & \dfrac{\partial f_2}{\partial \Delta\alpha} \end{bmatrix} \tag{44}$$

It is observed that $\Delta\dot{w}' = \Delta\dot{w}'(\delta\dot{w}, \Delta\alpha, \Delta t_1, \Delta t_2)$ and that the temporal variables Δt_i, $i = 1, 2$ are also dependent of the perturbations $\Delta t_i = \Delta t_i(\Delta\dot{w}, \Delta\alpha)$. Thus, the derivatives in (44) are expressed in the following manner

$$\frac{\partial f_i}{\partial u_j} = \frac{\partial f_i}{\partial u_j} + \frac{\partial f_i}{\partial \Delta t_1}\frac{\partial \Delta t_1}{\partial u_j} + \frac{\partial f_i}{\partial \Delta t_2}\frac{\partial \Delta t_2}{\partial u_j} \tag{45}$$

The derivatives $\partial\Delta t_i/\partial u_j$, $i, j = 1, 2$ are computed with the help of the implicit function theorem; to this end, new functions expressing the periodicity conditions of the perturbated system are introduced as

$$\begin{array}{l} h(\Delta\dot{w}, \Delta\alpha, \Delta t_1) = \tilde{w}_1\left(\dfrac{\pi}{\omega_c} + \Delta t_1\right) + \Delta = 0 \\ g(\Delta\dot{w}, \Delta\alpha, \Delta t_1, \Delta t_2) = \tilde{w}_1\left(\dfrac{\pi}{\omega_c} + \Delta t_1 + \Delta t_2\right) - \Delta = 0 \end{array} \tag{46}$$

Using (46), supposing that $(\partial h/\partial(\Delta t_1))_{(0,0,0)} \neq 0$ and $(\partial g/\partial(\Delta t_2))_{(0,0,0,0)} \neq 0$ the derivatives are expressed by [37, 39]

$$\begin{array}{l} \dfrac{\partial \Delta t_1}{\partial u_j} = -\dfrac{\partial h}{\partial u_j} \Big/ \left(\dfrac{\partial h}{\partial \Delta t_1}\right) \\ \dfrac{\partial \Delta t_2}{\partial u_j} = -\left(\dfrac{\partial g}{\partial u_j} + \dfrac{\partial g}{\partial \Delta t_1}\dfrac{\partial \Delta t_1}{\partial u_j}\right) \Big/ \left(\dfrac{\partial g}{\partial \Delta t_2}\right) \end{array} \tag{47}$$

An example of SIM is depicted in Fig. 4 for $R = 0.65$, $r = 0.5$ and $\Delta = 0.15$. The SIM is composed of two branches, the left branch is completely unstable and the right one is

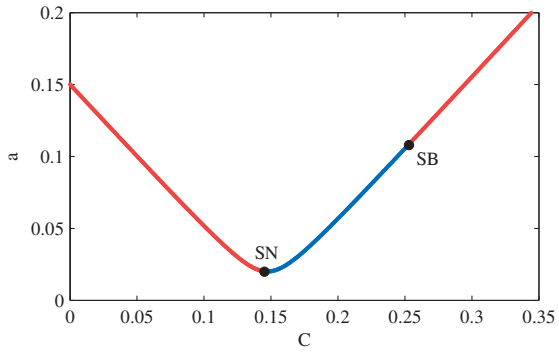

Figure 4: SIM of the coupled system at $1:1$ resonance for parameters $R = 0.65$, $r = 0.5$ and $\Delta = 0.15$. Blue (red) lines denote stable (unstable) solutions. SN and SB stand for saddle node and symmetry breaking, respectively.

partially stable. When the amplitude of the oscillation increases, a symmetry breaking bifurcation occurs and the regimes of motion with two symmetric impacts per cycle is destroyed.

4.1.2. Order ϵ^2, ϵ^3

Equation (25) at $O(\epsilon^2)$ is first analyzed. Substituting the solution of v_1 (28) into (25) gives

$$\begin{aligned} D_0^2 v_2 + 2\mu_1 D_0 v_2 + v_2 + \psi_c \left(v_2 - v_{2\tau}\right) = \left[-2\mu_1 - 2i\omega_c - \psi_c \tau \mathrm{e}^{-i\omega_c \tau}\right] D_1 A \mathrm{e}^{i\omega_c T_0} \\ + A^2 \mathrm{e}^{2i\omega_c T_0} \left(1 - \mathrm{e}^{-i\omega_c \tau}\right)^2 + 2A\bar{A}\left(1 - \mathrm{e}^{-i\omega_c \tau}\right) \end{aligned} \tag{48}$$

The condition of elimination of secular terms in (48) reads

$$\begin{aligned} &\left(-2\mu_1 - 2i\omega_c - \psi_c \tau \mathrm{e}^{-i\omega_c \tau}\right) D_1 A = 0 \\ &\rightarrow A(T_1, T_2) = A(T_2) \end{aligned} \tag{49}$$

which means that the slow modulation amplitude A does not depends on time scale T_2. Taking into account (49), the particular solution of v_2 is given by

$$v_2 = \psi_c \eta_1 \left(A^2 \Xi^2 \mathrm{e}^{2i\omega_c T_0} \Gamma^{-1} + 2A\bar{A}\Xi\right) + cc \tag{50}$$

where Ξ and Γ are constants defined as follow

$$\begin{aligned} \Gamma &= \left[-4\omega_c^2 + 4i\mu_1\omega_c + 1 + \psi_c\right) \mathrm{e}^{2i\omega_c \tau} - \psi_c \\ \Xi &= 1 - \mathrm{e}^{i\omega_c \tau} \end{aligned} \tag{51}$$

Equation (26) at $O(\epsilon^3)$ is now analyzed. In order to identify terms that produce secular terms, the expression of w_1 given in Eq. (30) is developed in Fourier series as

$$w_1 = \left(\frac{1}{2}\left(\Delta - C\right) + \frac{i\delta}{\pi} C\right) \mathrm{e}^{i\omega_c T_0} + \sum_{k=1}^{\infty} \frac{4C}{\pi^2 (2k-1)^2} \mathrm{e}^{(2k-1)i\omega_c T_0} + cc \tag{52}$$

Substituting Eqs. (28,52) and (50) into (26) gives

$$D_0^2 v_3 + 2\mu_1 D_0 v_3 + v_3 - \psi_c\left(v_{3\tau} - v_3\right) = \left\{D_2 A\left[-\psi_c \tau \mathrm{e}^{-i\omega_c \tau} - 2\mu_1 - 2i\omega_c\right]\right.$$
$$+\mu_1\omega_c\left[i(C-\Delta) + \frac{2\delta}{\pi}C + 2irA - \frac{8i}{\pi^2}C\right] - 2\psi_c^2\eta_1^2\bar{A}A^2\Xi^2\frac{\left(\mathrm{e}^{i\omega_c\tau}+1\right)\left(\mathrm{e}^{i\omega_c\tau}-1\right)^2}{\Gamma\mathrm{e}^{2i\omega_c\tau}}$$
$$+3\psi_c\eta_2 A^2\bar{A}\frac{\left(\mathrm{e}^{i\omega_c\tau}-1\right)^3}{\mathrm{e}^{2i\omega_c\tau}} + \frac{1+\psi_c}{2}\left[-\Delta + 2rA - \frac{8C}{\pi^2} - \frac{2iC\delta}{\pi} + C\right]\left(1-\mathrm{e}^{-i\omega_c\tau}\right)$$
$$\left.-2\sigma A\left(1-\mathrm{e}^{i\omega_c\tau}\right)\right\}\mathrm{e}^{i\omega_c T_0} + cc + NST \quad (53)$$

where NST denotes terms that do not produce secular terms. Secular terms are eliminated from (53) if

$$D_2 A\left[-\psi_c \tau \mathrm{e}^{-i\omega_c \tau} - 2\mu_1 - 2i\omega_c\right]$$
$$+\mu_1\omega_c\left[i(C-\Delta) + \frac{2\delta}{\pi}C + 2irA - \frac{8i}{\pi^2}C\right] - 2\psi_c^2\eta_1^2\bar{A}A^2\Xi^2\frac{\left(\mathrm{e}^{i\omega_c\tau}+1\right)\left(\mathrm{e}^{i\omega_c\tau}-1\right)^2}{\Gamma\mathrm{e}^{2i\omega_c\tau}}$$
$$+3\psi_c\eta_2 A^2\bar{A}\frac{\left(\mathrm{e}^{i\omega_c\tau}-1\right)^3}{\mathrm{e}^{2i\omega_c\tau}} + \frac{1+\psi_c}{2}\left[-\Delta + 2rA - \frac{8C}{\pi^2} - \frac{2iC\delta}{\pi} + C\right]\left(1-\mathrm{e}^{-i\omega_c\tau}\right)$$
$$-2\sigma A\left(1-\mathrm{e}^{i\omega_c\tau}\right) = 0 \quad (54)$$

Writing A in polar form $A = ae^{i\alpha}$ and splitting into real and imaginary parts, the equation governing the evolution of the amplitude of the lathe tool with respect to time scales T_2 is obtained as

$$D_2 a = c_1 a + c_2 a^3 + C\left(c_3\cos\alpha + c_4\sin\alpha\right) + c_5\cos\alpha + c_6\sin\alpha \quad (55)$$

where the coefficients c_i are complicated (which do not need to be explicitly stated at this stage of the analysis in order to follow the procedures involved in the expansion). Since the behavior of the system on the stable branch of the SIM is analyzed, the trigonometric relations given in Eq. (35) are substituted into (55) and the obtained equation is multiplied by $a(T_2)$, yielding

$$D_2 N = c_1' N + c_2' N^2 + c_3' C + c_4' C^2 + c_5' \quad (56)$$

where $N = a^2$. Fixed points are computed by vanishing the derivative in (56) and are given by

$$N = \frac{-c_1' \pm \sqrt{c_1'^2 - 4c_2'\left(c_3' C + c_4' C^2 + c_5'\right)}}{2c_2'} \quad (57)$$

Equation (57) constitutes an algebraic relation between the amplitude of the oscillations of the lathe tool and the vibro-impact NES. Therefore it can be viewed as the SIM of the problem at time scale T_3 when $T_2 \to \infty$ and the fixed points of the system are obtained graphically at the intersection of the SIM given in Eq. (36) and the curves (57), see [27].

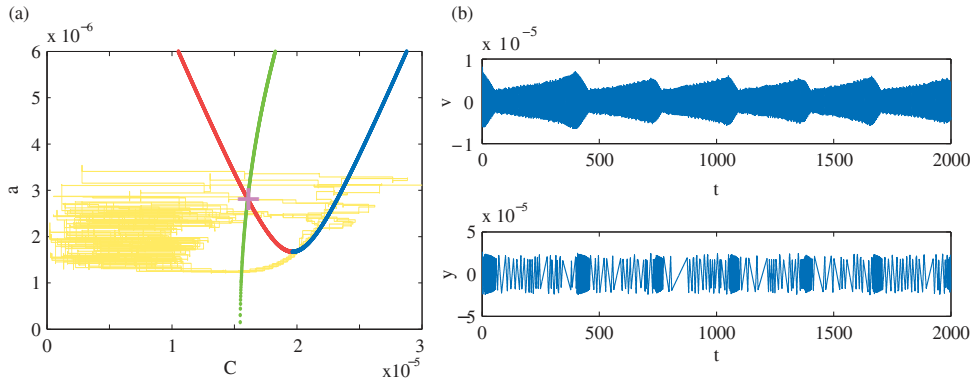

Figure 5: (a): $1:1$ SIM at time scales T_1 in blue (red) for stable (unstable) branch and T_3 in green for $\sigma = 1$. Pink + represents an unstable fixed points. Yellow lines represents the projection of the numerical integration on the SIM. (b): Result of numerical integration

4.2. Description of different response regimes

Different response regimes may be explained by studying the location of the fixed points on the SIM. The physical parameters of the primary system and the vibro-impact NES are given by

$$\epsilon^2 = 0.01, \quad \mu_1 = 0.03, \quad R = 0.65, \quad r = 0.8, \quad \Delta = 2.10^{-5} \tag{58}$$

The specific cutting coefficients ρ_i for the machining of steel are given in [36]

$$\begin{aligned} &\rho_1 = 6109.6\,10^6 Nm^{-2}, \quad \rho_2 = -54141.6\,10^9 Nm^{-3}, \\ &\rho_3 = 203769\,10^{12} Nm^{-4}, \quad h_0 = 1\,10^{-4} m \end{aligned} \tag{59}$$

The numerical integration is carried out on the zero order lobe for $\psi_c = 0.4$ (see Fig. 2). The step by step integration has been performed using the matlab *dde*23 algorithm together with the function *event* for the detection of the successive impacts.

4.2.1. Analog relaxation cycles

The SIM for $\sigma = 1$ depicted in Fig. 5(a). It is observed that an unstable fixed points is located on the unstable branch on the SIM while another unstable fixed point (not displayed here) is located on the unstable part of the right branch of the SIM (above the symmetry breaking bifurcation point). In this case, if the amplitude of the oscillations of the lathe tool became higher than the critical value a_{min} given in Eq. (37), the slow flow will be able to be attracted by the stable branch of the SIM. In this case, the vibro-impact NES will be synchronized with the lathe tool and will oscillate with two symmetric impacts per cycle. During the synchronized regimes, the energy of the system will be dissipated by successive impacts ($R < 1$) and the amplitude of the oscillations of the lathe tool will decrease until reaching the singular point a_{min}. At this point, the vibro-impact NES will escape the resonance capture and the amplitude of motion of the primary system will increase again, and so on.

The results of numerical integration depicted in Fig. 5(b) confirm the theoretical predictions; the amplitude of the oscillations of the lathe tool increase while the vibro-impact NES perform chaotic oscillations until the flow is attracted to the stable branch

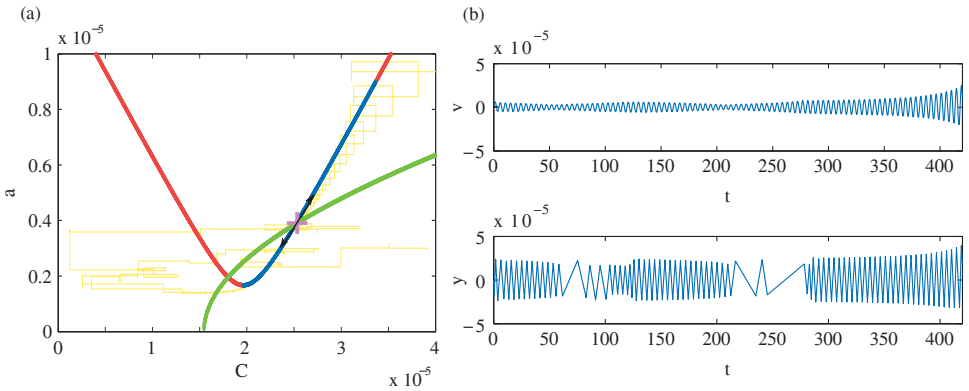

Figure 6: (a): $1:1$ SIM at time scales T_1 in blue (red) for stable (unstable) branch and T_3 in green for $\sigma = 4.6$. Pink + represents an unstable fixed points. Yellow lines represents the projection of the numerical integration on the SIM. (b): Result of numerical integration

of the SIM. Then, the amplitude of the primary system quickly decrease until the vibro-impact NES escape resonance capture. These cycle may be viewed as the analogy of the SMR regimes occurring in NES with cubic stiffness nonlinearities, but with a significant difference. In the case of NES with cubic stiffness, these cycles corresponds to jumps between the two stable branches of the SIM [20], while in this case they corresponds to successive synchronization and escapes of the synchronized regimes.

4.2.2. Limit of the passive control of chatter

When the value of σ is increased, the unstable fixed point located on the right branch of the SIM comes down along this branch as seen in Fig. 6(a) for $\sigma = 4.6$. If during the relaxation cycle, when the slow flow jump to the stable branch of the SIM, the landing point is above the saddle point, the slow flow will be repelled to higher amplitude and the system is no more controlled. The result of numerical integration, presented in Fig. 6(b), illustrates the theoretical prediction; after two relaxation cycle, the slow flow jump back to the stable branch of the SIM in the vicinity of the saddle point and the amplitude of the oscillation growth. In addition, it can be observed on the numerical integration, that when the amplitude of the oscillation growth sufficiently, the oscillation becomes unsymmetric (around $t = 400$), which is in agreement with the stability analysis of the SIM.

5. Experimental analysis

In order to validate experimentally the efficiency of a vibro-impact NES to passively controlling the chatter instability in turning, an experimental setup has been built.

5.1. Experimental setup

The trials have been realized on a Cazeneuve lathe (CT210) and the full experimental setup is depicted in Fig. 7. The machining operations have been carried out on a $40mm$ diameter, $XC38$ steel bar hold in the mandrel and the tail-stock. The cutting tool is a

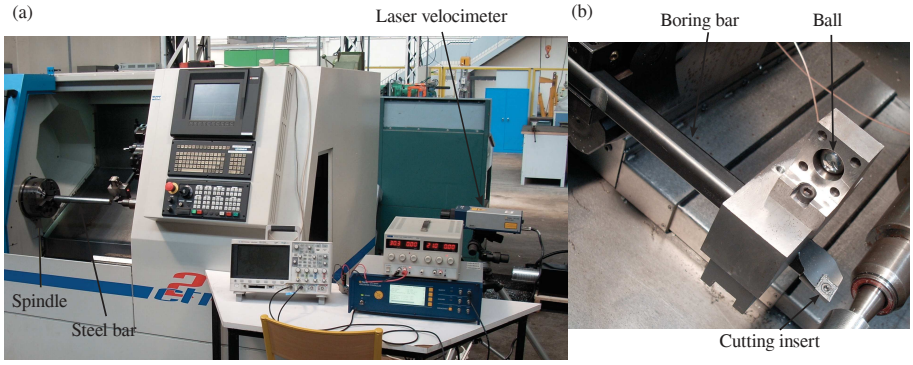

Figure 7: Experimental setup. (a) Global view, (b) detailed view of the boring bar with the embedded vibro-impact NES.

$250mm$ long boring bar which has been softened in one direction close to the tool holder to favour the bending mode in the cutting direction. In addition, a mass has been added on the tool tip in order to reduce the natural frequency of the first bending mode. The same feed-rate $h_0 = 0.1mm/tr$ is used for all the trials which consist in different turning passes with different spindle speed and depth of cut.

The oscillations of the tool tip have been measured using a laser vibrometer, and the specific cutting coefficients are those from [36]. The dynamics characteristics of the tool have been obtained by hammer testing and are summarized in Table 1. It can be noticed that the natural frequency is still high in comparison to other NES application, which is an interesting feature.

Table 1: Characteristics of the experimental setup

m_1	$3.1\,kg$	μ_1	$3\,\%$
f_1	$99.4\,Hz$	m_2	$32\,g$
r	0.8		

5.2. Validation of the stability lobe without NES

At first, experiments were performed without the vibro-impact NES in order to compare the behavior to the one identified theoretically on the linear analysis. The determination of the stable or unstable character of the process may not be straightforward due to the presence of strong forced vibration which can be due to an eccentricity of the workpiece, or when the spindle speed is close to the natural frequency of the lathe tool. In such case, the direct time series of the measurement may not be sufficient to identify chatter vibrations. To this end, simple signal processing method may be applied, such as re-sampling the signal at the spindle speed frequency [8]; in this case, a stable behavior will be represented by a straight line, because the relative position of the tool and the workpiece is always the same at each tool-path, whereas an unstable behavior will present a disorder. Another method consist in analyzing the pseudo-Poincaré section of

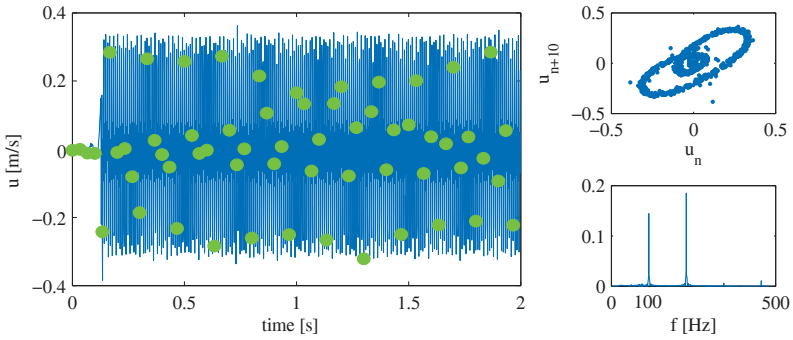

Figure 8: Analysis of an unstable trials at $s = 1800rpm, p = 0.1mm$ (corresponding to $\psi = 0.12, \Omega = 0.307$). (a) Blue lines : time history, green dots : re-sampled signal at the spindle frequency; (b) pseudo-Poincaré section; (c) frequency spectrum.

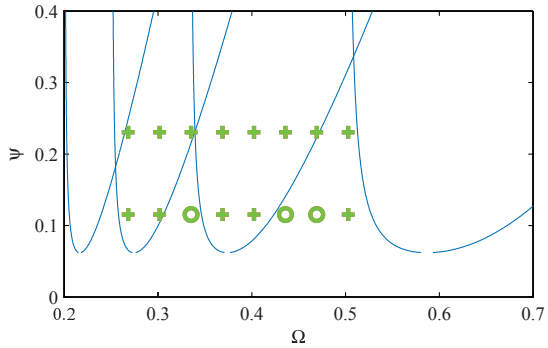

Figure 9: Theoretical and experimental stability chart. green cross and circle represents unstable and stable trials, respectively.

the measured signal. A stable behavior will present an attractor of type point, whereas an unstable behavior will present an attractor of type circle. An example of the analysis of an unstable trial is depicted in Fig. 8.

The comparison between the stability lobes obtained theoretically and those obtained experimentally is presented in Fig. 9. The stable (unstable) cutting conditions are represented by green circle (cross). The theoretical and experimental results are in agreement even if a shift on the left of the stability boundary is observed.

5.3. Sizing of the vibro-impact NES

Only the gap of the vibro-impact NES may be precisely adjusted during the fabrication process. The coefficient of restitution R may be varied using different materials couple for the ball and the cover. Here, a bearing ball and steel cover were used. Typical values of the amplitude of the oscillation measured during unstable trials without the vibro-impact NES were around $0.15mm$. The activation level of the vibro-impact NES computed with the help of Eq. (37) has been fixed to 50% of this value, which gives a gap $\Delta = 0.34mm$. After fabrication, the measured gap was $\Delta_{exp} = 0.32mm$.

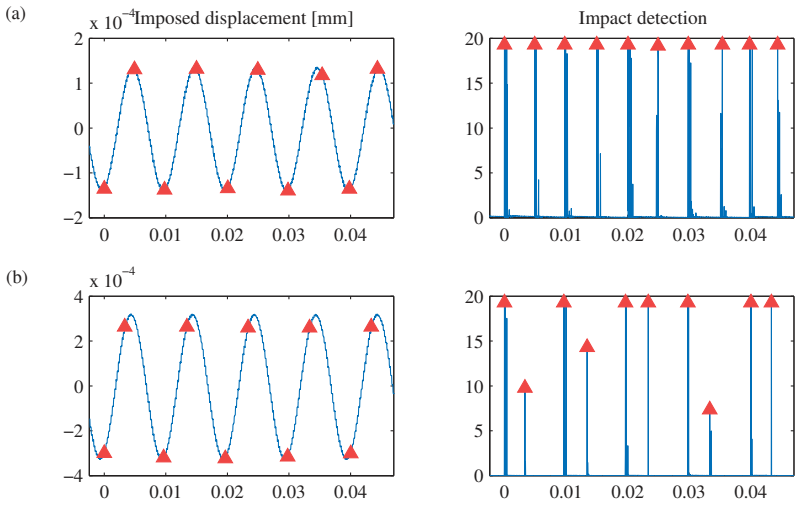

Figure 10: Time measurement for the experimental identification of the stable branch of the SIM, red triangles corresponds to the detected impacts for (a) $a = 7.66.10^{-5}$ and (b) $a = 1.81.10^{-4}$.

In order to check whether the activation level fit the theoretical prediction and to estimate the coefficient of restitution, the vibro-impact NES alone has been embedded on an electrodynamic shaker. In effect, this configuration corresponds to an harmonically forced vibro-impacts oscillator as in Eq. (29). So, it is possible to identified experimentally the stable branch of the SIM, which is very interesting for the sizing procedure. A base displacement at frequency $99.4Hz$, which correspond to the chatter frequency, is imposed to the vibro-impact NES and the successive impacts of the free mass on the cover are identified using accelerometers. Raw signals of two measurements are presented in Fig. 10. It is observed that in Fig. 10(a), for $a = 7.66.10^{-5}$, that the vibro-impact NES exhibit two symmetric impacts per cycle, that is, the time between two consecutive impacts is the same, while in Fig. 10(b), for $a = 1.81.10^{-4}$, there is still two impacts per cycle, but the time between two consecutive impacts differ, indicating asymmetric response.

The theoretical and experimental SIM are depicted in Fig. 11. Where the green circle corresponds to the experimental measurements, the continuous pink line denotes the experimentally identified activation level and the dashed pink line indicate the amplitude at which first asymmetric solutions have been observed. The value of coefficient of restitution of impact has been estimated by fitting the experimental results with the theoretical expression of the SIM given in Eq. (36); which give $R = 0.6$. Effectively, using coefficients of restitution from the literature for a plane-ball, steel-steel contact which is around 0.95 yields to erroneous results.

The experimentally identified activation level is slightly higher than the theoretical predictions, which is certainly due to the simplified model of the behavior of the free mass of the vibro-impact NES which do not capture its complex dynamics. The results are however in satisfactory agreement, and asymmetric solutions have also been observed, consistently with theoretical predictions.

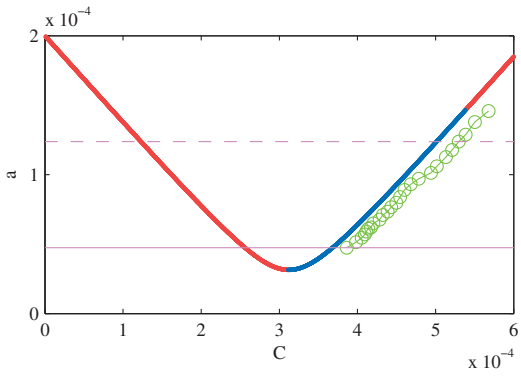

Figure 11: Theoretical and experimental SIM. Red and blue lines represents the unstable and stable branch of the SIM, respectively. Green circles represents the measurements points, continuous pink lines represents the experimentally determined level of activation and pink dotted lines the amplitude at which oscillations are no more symmetric

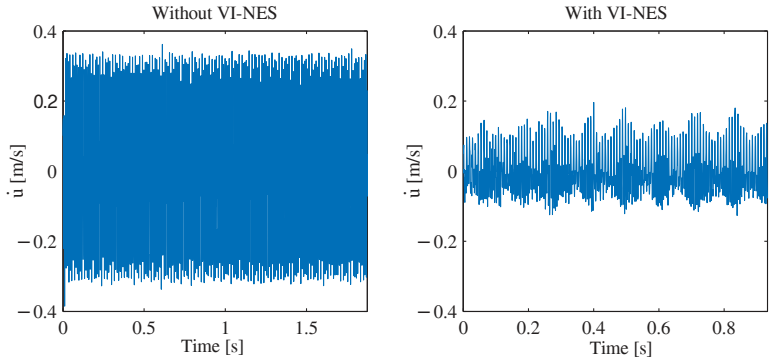

Figure 12: Comparison of the behavior during unstable machining operation without and with vibro-impact NES for $s = 1800rpm$ and $p = 0.1mm$ ($\psi = 0.12$ and $\Omega = 0.307$).

5.4. Passive control of chatter with a vibro-impact NES

In order to analyze experimentally the efficiency of the vibro-impact NES to mitigate chatter instability on turning process, trials with the vibro-impact NES embedded on the lathe tool on the unstable zone have been carried out. Two trials with and without vibro-impact NES are depicted in Fig. 12 for $s = 1800rpm$ and $p = 0.1mm$ ($\psi = 0.12$ and $\Omega = 0.307$).

It is observed that the presence of the vibro-impact NES changes drastically the behavior of the system. For the trial without vibro-impact NES, a constant high amplitude was measured whereas for the trial with vibro-impact NES, modulated response with moderate amplitude is observed. The measured modulated response is very similar to the analog relaxation cycle described theoretically. The successive impacts of the ball of the vibro-impact NES were clearly audible, however, the ambient noise due to machining operation did not allow us to measure the impact of the free-mass of the vibro-impact NES with the accelerometer. This behavior is however very promising, since a reduction of almost 50% on the vibration amplitude is observed.

6. Conclusion

This paper investigated the possibility of controlling the chatter instability, which may occur during machining operations, using a NES. Due to practical reasons, a vibro-impact type NES was preferred to the classic NES with cubic stiffness.

The coupled system has been analyzed using the method of multiple scales. At the first order of approximation, the expression of the SIM has been obtained. The stability analysis of its different branches was also performed. At the next order of approximation, the fixed points of the system are obtained at the intersection of the slow and super-slow invariant manifolds.

The analysis of the different response regimes allow us to reveal a control mechanism which may be viewed as the analogy of the SMR response observed in the case of NES with cubic stiffness. In this case, the vibro-impact NES enter in successive resonance capture with the lathe-tool and the energy is dissipated during these synchronous motion.

An experimental setup which consist in a lathe tool with an embedded vibro-impact NES has been presented. First trials without vibro-impact NES were performed to confirm the stable or unstable nature of the process for different cutting conditions. The activation level of the vibro-impact NES was chosen in accordance with these trials. Notice that the natural frequency of the tool (which is close to the chatter frequency) is $99.4\,Hz$ which is particularly high for NES application.

Due to the complicated real dynamics of the vibro-impact NES an original experimental procedure has been designed to validate the tuning of the NES. This procedure enable to identify experimentally the stable branch of the SIM.

Finally, two trials without and with the vibro-impact NES have been compared an promising results were obtained with a significant reduction of the amplitude of the tool. A deeper experimental investigation is left for further studies.

References

[1] M. Wiercigroch, Chaotic vibration of a simple model of the machine tool-cutting process system, Journal of Vibration and Acoustics 119 (3) (1997) 468–475.

[2] J. Warmiński, G. Litak, M. Cartmell, R. Khanin, M. Wiercigroch, Approximate analytical solutions for primary chatter in the non-linear metal cutting model, Journal of Sound and Vibration 259 (4) (2003) 917–933.

[3] S. Tobias, W. Fishwick, Theory of regenerative machine tool chatter, The engineer 205 (7) (1958) 199–203.

[4] Y. Altintas, E. Budak, Analytical prediction of stability lobes in milling, CIRP Annals-Manufacturing Technology 44 (1) (1995) 357–362.

[5] E. Gourc, S. Seguy, L. Arnaud, Chatter milling modeling of active magnetic bearing spindle in high-speed domain, International Journal of Machine Tools and Manufacture 51 (12) (2011) 928–936.

[6] F. A. Khasawneh, O. A. Bobrenkov, B. P. Mann, E. A. Butcher, Investigation of period-doubling islands in milling with simultaneously engaged helical flutes, Journal of Vibration and Acoustics 134 (2) (2012) 021008.

[7] B. Patel, B. Mann, K. Young, Uncharted islands of chatter instability in milling, International Journal of Machine Tools and Manufacture 48 (1) (2008) 124–134.

[8] B. Mann, T. Insperger, P. Bayly, G. Stépán, Stability of up-milling and down-milling, part 2: experimental verification, International Journal of Machine Tools and Manufacture 43 (1) (2003) 35–40.

[9] M. Mousseigne, Y. Landon, S. Seguy, G. Dessein, J.-M. Redonnet, Predicting the dynamic behaviour of torus milling tools when climb milling using the stability lobes theory, International Journal of Machine Tools and Manufacture 65 (2013) 47–57.

[10] S. Seguy, L. Arnaud, T. Insperger, Chatter in interrupted turning with geometrical defects: an industrial case study, The International Journal of Advanced Manufacturing Technology 75 (1) (2014) 45–56.
[11] A. Nayfeh, N. Nayfeh, Analysis of the cutting tool on a lathe, Nonlinear Dynamics 63 (3) (2011) 395–416.
[12] S. Seguy, T. Insperger, L. Arnaud, G. Dessein, G. Peigné, Suppression of period doubling chatter in high-speed milling by spindle speed variation, Machining Science and Technology 15 (2) (2011) 153–171.
[13] A. Matsubara, M. Maeda, I. Yamaji, Vibration suppression of boring bar by piezoelectric actuators and lr circuit, CIRP Annals-Manufacturing Technology 63 (1) (2014) 373–376.
[14] C. Brecher, D. Manoharan, U. Ladra, H.-G. Köpken, Chatter suppression with an active workpiece holder, Production engineering 4 (2-3) (2010) 239–245.
[15] N. Sims, Vibration absorbers for chatter suppression: a new analytical tuning methodology, Journal of Sound and Vibration 301 (3) (2007) 592–607.
[16] M. Wang, T. Zan, Y. Yang, R. Fei, Design and implementation of nonlinear tmd for chatter suppression: An application in turning processes, International Journal of Machine Tools and Manufacture 50 (5) (2010) 474–479.
[17] M. Wang, Feasibility study of nonlinear tuned mass damper for machining chatter suppression, Journal of Sound and Vibration 330 (9) (2011) 1917–1930.
[18] Y. Yang, J. Munoa, Y. Altintas, Optimization of multiple tuned mass dampers to suppress machine tool chatter, International Journal of Machine Tools and Manufacture 50 (9) (2010) 834–842.
[19] A. Vakakis, O. Gendelman, Energy pumping in nonlinear mechanical oscillators: part iiresonance capture, Journal of Applied Mechanics 68 (1) (2001) 42–48.
[20] Y. Starosvetsky, O. Gendelman, Strongly modulated response in forced 2dof oscillatory system with essential mass and potential asymmetry, Physica D: Nonlinear Phenomena 237 (13) (2008) 1719–1733.
[21] E. Gourc, G. Michon, S. Seguy, A. Berlioz, Experimental investigation and design optimization of targeted energy transfer under periodic forcing, Journal of Vibration and Acoustics 136 (2) (2014) 021021.
[22] C.-H. Lamarque, O. Gendelman, A. Savadkoohi, E. Etcheverria, Targeted energy transfer in mechanical systems by means of non-smooth nonlinear energy sink, Acta mechanica 221 (1-2) (2011) 175–200.
[23] A. Savadkoohi, C.-H. Lamarque, Z. Dimitrijevic, Vibratory energy exchange between a linear and a nonsmooth system in the presence of the gravity, Nonlinear Dynamics 70 (2) (2012) 1473–1483.
[24] F. Nucera, A. Vakakis, D. McFarland, L. Bergman, G. Kerschen, Targeted energy transfers in vibro-impact oscillators for seismic mitigation, Nonlinear Dynamics 50 (3) (2007) 651–677.
[25] F. Nucera, F. Lo Iacono, D. McFarland, L. Bergman, A. Vakakis, Application of broadband nonlinear targeted energy transfers for seismic mitigation of a shear frame: Experimental results, Journal of Sound and Vibration 313 (1) (2008) 57–76.
[26] O. Gendelman, Analytic treatment of a system with a vibro-impact nonlinear energy sink, Journal of Sound and Vibration 331 (21) (2012) 4599–4608.
[27] O. Gendelman, T. Bar, Bifurcations of self-excitation regimes in a van der pol oscillator with a nonlinear energy sink, Physica D: Nonlinear Phenomena 239 (3-4) (2010) 220–229.
[28] Y. Lee, A. Vakakis, L. Bergman, D. McFarland, G. Kerschen, Suppression aeroelastic instability using broadband passive targeted energy transfers, part 1: Theory, AIAA Journal 45 (3) (2007) 693–711.
[29] Y. Lee, G. Kerschen, D. McFarland, W. Hill, C. Nichkawde, T. Strganac, L. Bergman, A. Vakakis, Suppressing aeroelastic instability using broadband passive targeted energy transfers, part 2: experiments, AIAA Journal 45 (10) (2007) 2391–2400.
[30] B. Vaurigaud, L. Manevitch, C.-H. Lamarque, Passive control of aeroelastic instability in a long span bridge model prone to coupled flutter using targeted energy transfer, Journal of Sound and Vibration 330 (11) (2011) 2580–2595.
[31] R. Viguié, G. Kerschen, J.-C. Golinval, D. McFarland, L. Bergman, A. Vakakis, N. van de Wouw, Using passive nonlinear targeted energy transfer to stabilize drill-string systems, Mechanical Systems and Signal Processing 23 (1) (2009) 148–169.
[32] E. Gourc, S. Seguy, G. Michon, A. Berlioz, Delayed dynamical system strongly coupled to a nonlinear energy sink: application to machining chatter, in: International Conference on Structural Nonlinear Dynamics and Diagnostics, 2012.
[33] A. Nankali, H. Surampalli, Y. Lee, T. Kalmar-Nagy, Suppression of machine tool chatter using non-

linear energy sink, in: Proceedings of ASME-IDETC, 2011.
[34] A. Nankali, H. Surampalli, Y. Lee, T. Kalmar-Nagy, Targeted energy transfer for suppressing regenerative instabilities in a 2-dof machine tool model, in: Proceedings of ASME-IDETC, 2013.
[35] H. Shi, S. Tobias, Theory of finite amplitude machine tool instability, International Journal of Machine Tool Design and Research 24 (1) (1984) 45–69.
[36] Z. Dombovari, D. Barton, E. Wilson, G. Stepan, On the global dynamics of chatter in the orthogonal cuttingmodel, International Journal of Non-Linear Mechanics 46 (1) (2011) 330–338.
[37] Y. Yue, J. Xie, Symmetry and bifurcations of a two-degree-of-freedom vibro-impact system, Journal of Sound and Vibration 314 (1) (2008) 228–245.
[38] S. Lenci, G. Rega, Periodic solutions and bifurcations in an impact inverted pendulum under impulsive excitation, Chaos, Solitons & Fractals 11 (15) (2000) 2453–2472.
[39] G. Luo, J. Xie, S. Guo, Periodic motions and global bifurcations of a two-degree-of-freedom system with plastic vibro-impact, Journal of sound and vibration 240 (5) (2001) 837–858.